

AAS 11-466



# **RELATIVE MOTION CONTROL FOR TWO-SPACECRAFT ELECTROSTATIC ORBIT CORRECTIONS**

**Erik A. Hogan, and Hanspeter Schaub**

## **AAS/AIAA Astrodynamics Specialists Conference**

**Girdwood, Alaska**

**July 31–August 4, 2011**

**AAS Publications Office, P.O. Box 28130, San Diego, CA 92198**

# RELATIVE MOTION CONTROL FOR TWO-SPACECRAFT ELECTROSTATIC ORBIT CORRECTIONS

Erik A. Hogan\*, and Hanspeter Schaub†

The charged relative motion dynamics and control of a two-craft system is investigated if one vehicle is performing a low-thrust orbit correction using inertial thrusters. The nominal motion is an along-track configuration where active electrostatic charge control is maintaining an attractive force between the two vehicles. In this study the charging is held fixed, and the inertial thruster of the tugging vehicle is controlled to stabilize the relative motion to a nominal fixed separation distance. Using a candidate Lyapunov function, the relative orbit control law of the tugging vehicle with respect to the passive vehicle is shown to be asymptotically stable. Analysis of the control system gains is performed in order to achieve a desired settling time and damping ratio. The effects of uncertainties in the vehicle charges are also examined. Using numerical simulation, the performance of the proposed control system is investigated for a formation in GEO. Results obtained from integration of the relative equations of motion are compared to full inertial simulations.

## INTRODUCTION

Electrostatic force actuation for spacecraft formation control is a concept that is gaining significant attention in the field of formation flying.<sup>1,2</sup> In these Coulomb formations, active charge control is applied to generate specified inter-craft electrostatic forces that are used to manipulate the relative positions of the nodes within the formation.<sup>3</sup> In the presence of perturbations, such as differential gravity, these forces may be used to maintain coherence of multiple craft in close proximity.<sup>4</sup> Electrostatic forces have also been proposed as a method to inflate a tethered structure where individual nodes of a formation are connected by physical tethers such as cables.<sup>5,6</sup>

The prior work on charged relative motion dynamics of clusters of spacecraft only considers the relative motion control of a non-perturbed system.<sup>4,7,8</sup> The active charge control is expected to be extremely fuel efficient ( $I_{sp}$  values as high as  $10^9 - 10^{12}$  seconds) and require small, Watt levels of electrical power to operate.<sup>9</sup> These concepts assume separation distances on the order of dozens of meters. However, an unexplored research area is how do such Coulomb spacecraft clusters perform orbit corrections. In particular, if only a sub-set of cluster elements perform inertial thrusting, then the passive cluster elements must be tugged along with the electrostatic forces. Of interest is how can the charged relative motion dynamics be stabilized, without resulting in collisions of the cluster members, while a low-thrust orbit correction is being engaged.

A related scenario is considered in Reference 10. Here the use of electrostatic forces to tug a space debris object into a disposal orbit is investigated. Using thrusters operating on the milliNewton

\*Graduate Student, Aerospace Engineering Sciences, University of Colorado at Boulder, Boulder, CO

†Associate Professor, H. Joseph Smead Fellow, Department of Aerospace Engineering Sciences, University of Colorado, 431 UCB, Colorado Center for Astrodynamics Research, Boulder, CO 80309-0431

level, the tug craft approaches and engages the debris object. Because the electrostatic forces do not require a physical tether to exist between tug and target, the debris object can be reorbited without requiring any physical contact. Once the electrostatic force is active between the tug and debris, the tug utilizes low-thrust to slowly pull the debris into a disposal orbit. Reference 10 considers the effort required to achieve a disposal orbit, and investigates how the debris orbital elements change with time under the influence of the tug. Reference 10 does not, however, consider the relative motion of the two craft during the reorbiting maneuver; nor does it propose a feedback control system for maintaining the tug and debris object in the necessary relative positions.

The current work presents the first discussion on feedback stabilizing the charged relative motion while one cluster element is performing a low-thrust orbit correction. The relative equations of motion between a tug (or chief) craft and a secondary craft (called a deputy) are developed, and a control algorithm is proposed to maintain a desired relative position using inertial thrusting on the chief only. The applications of the current study include electrostatic debris reorbiting applications, as well as maintaining an observation craft in close proximity to a main craft that can provide real time visual information. If the main craft needs to reorbit as part of its mission requirements, it may do so with the observer in tow. The following developments are made in a general way, so as to be applicable to any charged two-craft formation in orbit, whether reorbiting a debris object or maintaining an observer in close proximity. Due to the limitations of the plasma shielding of electrostatic charge, the application of the electrostatic tether reorbiting concept focuses on spacecraft in or near geosynchronous orbit.

The paper is structured as follows. First, the fundamentals of relative dynamics with respect to a slowly accelerating Hill frame are provided. The relative dynamics of the two craft in the rotating Hill frame are developed considering gravitational, electrostatic, and thruster effects. Next, a spherical coordinate frame is introduced and the equations of motion are developed in this spherical frame. The spherical frame is then used to develop a control law using Lyapunov stability analysis. Consideration of desired settling times and the nature of damping in the system response is used to select gains for the controller. After that, the effects of uncertainties in the craft charges on the control system response are investigated. Finally, numerical simulation is used to illustrate the performance of the controller in maintaining the desired relative position of chief and deputy.

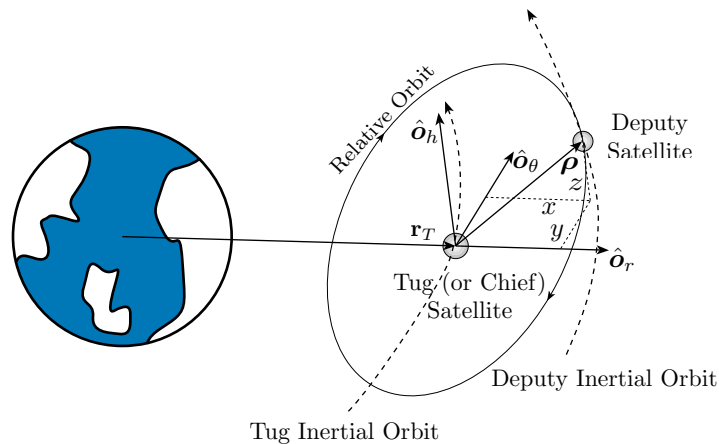


**Figure 1. Illustration of Tug Rectilinear LVLH or Hill Coordinate Frame**

## RELATIVE ORBITAL DYNAMICS DURING ORBIT CHANGE MANEUVER

### Hill Coordinate Frame

The Local-Vertical-Local-Horizontal (LVLH), often also referred to as the Hill coordinate frame, is briefly outlined in this section. A rectilinear Hill frame  $\mathcal{H} : \{\hat{\mathbf{o}}_r, \hat{\mathbf{o}}_\theta, \hat{\mathbf{o}}_h\}$  is attached to the tug (or chief) orbital position as illustrated in Figure 1. This rotating frame has its origin coincide with the tug center of mass, and the orientation is defined through

$$\hat{\mathbf{o}}_r = \frac{\mathbf{r}_T}{r_T}, \quad \hat{\mathbf{o}}_\theta = \hat{\mathbf{o}}_h \times \hat{\mathbf{o}}_r, \quad \hat{\mathbf{o}}_h = \frac{\mathbf{r}_T \times \dot{\mathbf{r}}_T}{|\mathbf{r}_T \times \dot{\mathbf{r}}_T|} \quad (1a)$$

where  $\mathbf{r}_T$  is the inertial position vector of the chief,  $\dot{\mathbf{r}}_T$  is the inertial velocity vector, and the shorthand notation  $r_T = |\mathbf{r}_T|$  is used.

The direction cosine matrix (DCM) of the Hill frame relative to an inertial frame, expressed through  $\mathcal{N} : \{\hat{\mathbf{n}}_1, \hat{\mathbf{n}}_2, \hat{\mathbf{n}}_3\}$ , is defined through<sup>11</sup>

$$[NH] = [\mathcal{N}\hat{\mathbf{o}}_r \quad \mathcal{N}\hat{\mathbf{o}}_\theta \quad \mathcal{N}\hat{\mathbf{o}}_h] \quad (2)$$

Let  $\boldsymbol{\omega}_{H/N}$  be the angular velocity of the Hill frame relative to the inertial frame, then Hill-frame centric deputy motion  ${}^{\mathcal{H}}\boldsymbol{\rho}$  is translated into inertial motion  ${}^{\mathcal{N}}\mathbf{r}_d$  using

$${}^{\mathcal{N}}\mathbf{r}_d = {}^{\mathcal{N}}\mathbf{r}_T + [NH] {}^{\mathcal{H}}\boldsymbol{\rho} \quad (3)$$

where

$${}^{\mathcal{H}}\boldsymbol{\rho} = \begin{bmatrix} x \\ y \\ z \end{bmatrix} \quad (4)$$

and  $(x, y, z)$  are the Hill-frame centric cartesian deputy position coordinates. The inertia and Hill-frame relative velocities are related using the transport theorem:<sup>11</sup>

$${}^{\mathcal{N}}\dot{\mathbf{r}}_d = {}^{\mathcal{N}}\dot{\mathbf{r}}_T + [NH] \left( \frac{d({}^{\mathcal{H}}\boldsymbol{\rho})}{dt} + {}^{\mathcal{H}}\boldsymbol{\omega}_{H/N} \times {}^{\mathcal{H}}\boldsymbol{\rho} \right) \quad (5)$$

where

$$\frac{d({}^{\mathcal{H}}\boldsymbol{\rho})}{dt} = {}^{\mathcal{H}}\boldsymbol{\rho}' = \begin{bmatrix} \dot{x} \\ \dot{y} \\ \dot{z} \end{bmatrix} \quad (6)$$

Note the use of the short-hand notation for Hill-frame dependent time derivatives:

$$\frac{{}^{\mathcal{H}}d(\boldsymbol{\rho})}{dt} \equiv \boldsymbol{\rho}' \quad (7)$$

## Relative Motion With Respect to a Constantly Accelerating Frame

Next the classical Hill frame relative orbital dynamics are revisited considering that the Hill frame is no longer on a circular orbit, but on a slowly spiraling trajectory. This study only investigates inertial thrusting to perform Semi-Major Axis (SMA) changes which require thrusting in the along-track direction.

The deputy and chief inertial position vectors are related through

$$\mathbf{r}_d = \mathbf{r}_T + \boldsymbol{\rho} \quad (8)$$

The relative motion  $\boldsymbol{\rho}$  is thus expressed through

$$\boldsymbol{\rho} = \mathbf{r}_d - \mathbf{r}_T \quad (9)$$

Note that this is a coordinate-frame independent vector formulation of the relative motion. Taking two inertial time derivatives of Eq. (9) yields

$$\ddot{\boldsymbol{\rho}} = \ddot{\mathbf{r}}_d - \ddot{\mathbf{r}}_T \quad (10)$$

The inertial chief or tug equations of motion are given through

$$\ddot{\mathbf{r}}_T = -\frac{\mu}{r_T^3}\mathbf{r}_T + \frac{\mathbf{F}_c}{m_T} + \mathbf{u}_T \quad (11)$$

where  $\mu$  is the gravitational constant, and  $m_T$  is the chief mass. The first term of the right hand side is the gravitational acceleration, while  $\mathbf{F}_c$  is the electrostatic force acting between tug and deputy, and  $\mathbf{u}_T$  is the net control acceleration being produced by the chief's inertial thrusters. The inertial deputy equations of motion are

$$\ddot{\mathbf{r}}_d = -\frac{\mu}{r_d^3}\mathbf{r}_d - \frac{\mathbf{F}_c}{m_d} \quad (12)$$

where  $m_d$  is the deputy mass.

Substituting Eqs. (12) and (11) into Eq. (10) yields the vector relative equations of motion

$$\ddot{\boldsymbol{\rho}} = -\frac{\mu}{r_d^3}\mathbf{r}_d + \frac{\mu}{r_T^3}\mathbf{r}_T - \frac{\mathbf{F}_c}{m_d} - \frac{\mathbf{F}_c}{m_T} - \mathbf{u}_T \quad (13)$$

Defining the control acceleration vector  $\mathbf{u}$  as

$$\mathbf{u} = -\mathbf{F}_c \left( \frac{m_T + m_d}{m_T m_d} \right) - \mathbf{u}_T \quad (14)$$

the relative EOM are rewritten as

$$\ddot{\boldsymbol{\rho}} = -\frac{\mu}{r_d^3}\mathbf{r}_d + \frac{\mu}{r_T^3}\mathbf{r}_T + \mathbf{u} \quad (15)$$

This algebraic form is equivalent now to the classical Clohessy-Wiltshire-Hill (CWH) equations of relative motion, where  $\mathbf{u}$  would be the deputy control acceleration. Note that the control acceleration  $\mathbf{u}$  contains both the impact of performing inertial thrusting, as well as the influence of

the electrostatic attraction. To obtain  $\ddot{\rho}$ , we need to take two inertial time derivatives. The inertial derivative of  $\rho$  is

$$\dot{\rho} = \rho' + \omega_{H/N} \times \rho \quad (16)$$

If the chief vehicle is on a circular orbit, then the orbital angular velocity vector is simply

$$\omega_{H/N} = n\hat{o}_h \quad (17)$$

where  $n = \sqrt{\mu/a^3}$  is the mean orbit rate, and  $a$  is the tug semi-major axis. However, because the tug is performing a low-thrust semi-major axis orbit change, the mean orbit rate  $n$  is not constant, but rather  $n = n(t)$  is a function of time. However, the deputy reorbiting is assumed to not change the orbit plane of the deputy because only the SMA is being changed. Thus, the orbit normal direction  $\hat{o}_h$  is inertially fixed, and the orbit angular velocity is written as

$$\omega_{H/N} = n(t)\hat{o}_h \quad (18)$$

Note that the tug can maneuver relative to the deputy a general way. Thus, if charge control is turned on during general three-dimensional relative motion, then small deputy orbit plane changes are possible. However, these variations are ignorable because the nominal configuration has the tug accelerating the deputy in the positive along-track direction. This configuration provides the most efficient means to increase the semi-major axis of the deputy, and thus raise its orbit altitude.

Taking the inertial derivative of Eq. (16) yields

$$\ddot{\rho} = \rho'' + 2\omega_{H/N} \times \rho' + \dot{\omega}_{H/N} \times \rho + \omega_{H/N} \times (\omega_{H/N} \times \rho) \quad (19)$$

For the CWH equations where the chief motion is circular the orbital angular acceleration  $\dot{\omega}_{H/N}$  is set to zero and dropped from this expression. For optimal SMA corrections, the along-track acceleration  $a_\theta$  of the deputy is given by

$$a_\theta = \frac{F_c}{m_d} \quad (20)$$

The orbit angular acceleration is then approximated as

$$\dot{n} = \frac{a_\theta}{r_d} \quad (21)$$

Knowing the actual along-track acceleration  $a_\theta$  it would be possible to include this term. In practice determining this orbital acceleration term is non-trivial because the tug-deputy system is not aligned with the along track direction at all times. Further, the orbital acceleration requires knowledge of the exact electrostatic force between the two bodies. This is can be very challenging to obtain in practice. However, as the following analysis shows, this acceleration is a very small term that be neglected for the purpose of modeling the slowly-accelerating relative motion dynamics. Thus, the question is for what electrostatic force levels  $F_c^*$  will  $\dot{n} \approx n^2$ . Using Eqs. (20) and (21) we find

$$\frac{F_c^*}{m_d r_d} = \dot{n} \approx n^2 \quad \Rightarrow \quad F_c^* = n^2 m_d r_d \quad (22)$$

Assuming a deputy craft with the mass  $m_d = 2000$  kg, and the geostationary orbit radius of about  $r_d = 42,000$  km, we obtain

$$\begin{aligned} n &= 7.335 \cdot 10^{-5} \text{ rad/s} \\ n^2 &= 5.3801 \cdot 10^{-9} \text{ rad/s} \end{aligned}$$

This leads to a critical acceleration force of

$$F_c^* = 451.9 \text{ N}$$

Because the expected electrostatic forces are expected to be in the milli-Newton range, the actual  $F_c$  are about 5 orders of magnitude smaller than this critical acceleration force. This justifies neglecting the difficult to measure  $\dot{\omega}_{H/N}$  in Eq. (19), resulting in the simplified relative motion acceleration expression

$$\ddot{\rho} = \rho'' + 2n(t)\hat{o}_h \times \rho' + n(t)^2\hat{o}_h \times (\hat{o}_h \times \rho) \quad (23)$$

using Eq. (18). Note that the orbit rate  $n(t)$  will decrease by about 1.1% as the deputy is reorbited from GEO to a 300 km larger super-synchronous orbit. Because the slowly varying orbit rate is easy to measure, it is kept as a time-dependent parameter in our relative equations of motion.

Next, let us refine the vector equations of motion in Eq. (7), which do not depend on a particular coordinate system, into the equivalent matrix form which provides the ordinary differential equations for the Hill frame coordinates  $(x, y, z)$ . Assuming  $\rho$  is much smaller than  $r_T$ , the differential gravity term is reduced to a linear form.<sup>11</sup> After linearizing the  $\ddot{\rho}$  term, a modified version of the classical CWH equations are obtained:

$$\ddot{x} - 2n(t)\dot{y} - 3n^2(t)x = u_x \quad (24a)$$

$$\ddot{y} + 2n(t)\dot{x} = u_y \quad (24b)$$

$$\ddot{z} + n^2(t)z = u_z \quad (24c)$$

Note that the constant mean orbit rate  $n$  of the CWH equations is replaced with the osculating  $n(t)$  orbit rate expression. The Coulomb forcing and inertial thrusting influence on the relative deputy motion with respect to the tug is embedded within the control acceleration  $u$  expressions.

### Relative Spherical Equations of Motion

The Cartesian form of the CW equations are not very convenient for the relative motion control development in that the rectilinear  $(x, y, z)$  coordinates couple both information regarding the separation distance as well as the relative orientation. Instead a set of spherical relative position coordinates  $(L, \theta, \phi)$  are employed where  $L$  is the center-to-center separation distance of the tug and deputy,  $\theta$  is the inplane rotation angle, and  $\phi$  is the out of plane rotation angle. The spherical coordinate frame  $\mathcal{S} : \{\hat{s}_L, \hat{s}_\theta, \hat{s}_\phi\}$  is illustrated in Figure 2.

The relative orientation angles  $\theta$  and  $\phi$  are a 3-2 Euler angle sequence with respect to the Hill frame  $\mathcal{H}$ . Carrying out the matrix multiplication leads to the DCM mapping from the Hill to the spherical frame:

$$[SH] = \begin{bmatrix} \cos(\phi(t)) \sin(\theta(t)) & -\cos(\theta(t)) \cos(\phi(t)) & -\sin(\phi(t)) \\ \cos(\theta(t)) & \sin(\theta(t)) & 0 \\ \sin(\theta(t)) \sin(\phi(t)) & -\cos(\theta(t)) \sin(\phi(t)) & \cos(\phi(t)) \end{bmatrix} \quad (25)$$

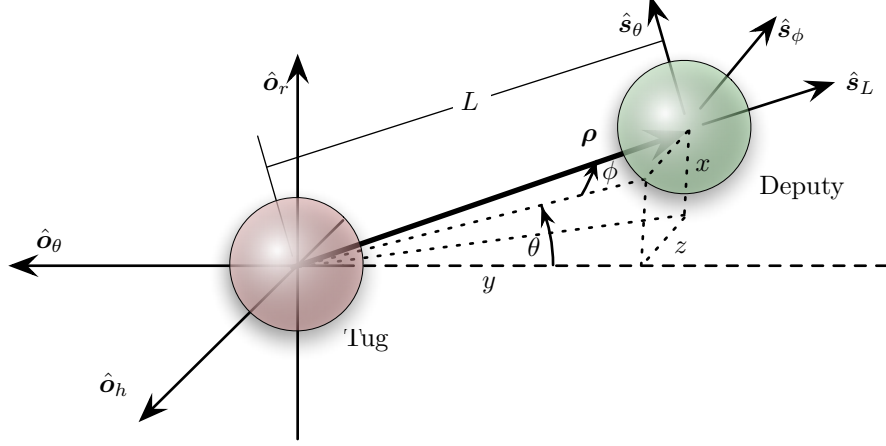


**Figure 2. Illustration of the Spherical  $S$  Coordinate Frame**

The  $S$  and  $\mathcal{H}$  position coordinates are related through:

$$L = \sqrt{x^2 + y^2 + z^2} \quad (26a)$$

$$\theta = \arctan\left(\frac{x}{-y}\right) \quad (26b)$$

$$\phi = \arcsin\left(\frac{-z}{L}\right) \quad (26c)$$

and

$$\begin{bmatrix} x \\ y \\ z \end{bmatrix} = [SH]^T \begin{bmatrix} L \\ 0 \\ 0 \end{bmatrix} = \begin{bmatrix} L \sin \theta \cos \phi \\ -L \cos \theta \cos \phi \\ -L \sin \phi \end{bmatrix} \quad (27)$$

The relative motion rate coordinates are related through:

$$\begin{bmatrix} \dot{L} \\ \dot{\theta} \\ \dot{\phi} \end{bmatrix} = \begin{bmatrix} \cos(\phi) \sin(\theta) & -\cos(\theta) \cos(\phi) & -\sin(\phi) \\ \frac{\cos(\theta) \sec(\phi)}{L} & \frac{\sec(\phi) \sin(\theta)}{L} & 0 \\ -\frac{\sin(\theta) \sin(\phi)}{L} & \frac{\cos(\theta) \sin(\phi)}{L} & -\frac{\cos(\phi)}{L} \end{bmatrix} \begin{bmatrix} \dot{x} \\ \dot{y} \\ \dot{z} \end{bmatrix} \quad (28)$$

and

$$\begin{bmatrix} \dot{x} \\ \dot{y} \\ \dot{z} \end{bmatrix} = \begin{bmatrix} \sin \theta \cos \phi & L \cos \theta \cos \phi & -L \sin \theta \sin \phi \\ -\cos \theta \cos \phi & L \sin \theta \cos \phi & L \cos \theta \sin \phi \\ -\sin \phi & 0 & -L \cos \phi \end{bmatrix} \begin{bmatrix} \dot{L} \\ \dot{\theta} \\ \dot{\phi} \end{bmatrix} \quad (29)$$

Substituting the kinematic transformations in Eqs. (27) and (29) into the rectilinear EOM in Eq. (24), and performing significant algebraic simplifications, leads to the following spherical relative equations of motion:

$$\begin{bmatrix} \ddot{L} \\ \ddot{\theta} \\ \ddot{\phi} \end{bmatrix} = [F(L, \theta, \phi, \dot{L}, \dot{\theta}, \dot{\phi})] + [G(L, \phi)]^S \mathbf{u} \quad (30)$$

where

$$\begin{aligned}
S_{\mathbf{u}} &= \begin{bmatrix} u_L \\ u_\theta \\ u_\phi \end{bmatrix} \\
[F] &= \begin{bmatrix} \frac{1}{4}L \left( n^2(t) (-6 \cos(2\theta) \cos^2(\phi) + 5 \cos(2\phi) + 1) + 4\dot{\theta} \cos^2(\phi) (2n(t) + \dot{\theta}) + 4\dot{\phi}^2 \right) \\ \left( 3n^2(t) \sin(\theta) \cos(\theta) + 2\dot{\phi} \tan(\phi) (n(t) + \dot{\theta}) \right) - 2\frac{\dot{L}}{L} (n(t) + \dot{\theta}) \\ \frac{1}{4} \sin(2\phi) \left( n^2(t) (3 \cos(2\theta) - 5) - 2\dot{\theta} (2n(t) + \dot{\theta}) \right) - 2\frac{\dot{L}}{L} \dot{\phi} \end{bmatrix} \\
[G] &= \begin{bmatrix} 1 & 0 & 0 \\ 0 & \frac{1}{L \cos \phi} & 0 \\ 0 & 0 & -\frac{1}{L} \end{bmatrix}
\end{aligned}$$

Note that due to the kinematics of spherical coordinates, this description is singular for large out-of-plane motions where  $\phi \rightarrow \pm\pi/2$ .

### Electrostatic Force Model

In order to implement the dynamic model, an expression for the electrostatic force between two craft is needed. Here, the two bodies will be treated as spheres. For an isolated sphere in a vacuum, the charge to voltage relationship is

$$V = k_T \frac{q}{R}, \quad (31)$$

where  $R$  is the sphere radius,  $q$  is the charge on the sphere, and  $k_T$  is the Coulomb constant. When another charged object is in close proximity, this voltage to charge relationship no longer holds, as the second object will affect the charge distribution on the first. In this application, the voltages on the craft are considered to be held at constant values.

The voltages on the two spherical craft are denoted as  $V_1$  and  $V_2$ . The potential on craft one is thus a function of the self capacitance in Eq. (31) and the potential due to the second sphere,<sup>12</sup>

$$V_1 = k_T \frac{q_1}{R_1} + k_T \frac{q_2}{L}. \quad (32)$$

The potential on craft two can be obtained in the same manner. The voltages on both spheres are linear functions of the charges, expressed as

$$\begin{bmatrix} V_1 \\ V_2 \end{bmatrix} = k_T \begin{bmatrix} \frac{1}{R_1} & \frac{1}{L} \\ \frac{1}{L} & \frac{1}{R_2} \end{bmatrix} \begin{bmatrix} q_1 \\ q_2 \end{bmatrix} \quad (33)$$

If the voltages on the spheres are held constant, the charges may be solved for at any point in time by inversion of Eq. (33).

This approach to charge determination given craft voltages is relatively new in the field of Coulomb formation flying, where craft have traditionally been treated as point charges. More information about using this position dependent capacitance model is given in Reference ?. Craft of arbitrary geometries will certainly not be perfect spheres. However, spherical models are more appropriate than point charge approximations as they allow for the effects of neighboring craft to be included in

the charge to voltage model. Furthermore, Reference ? provides a method for determining effective spheres for arbitrary craft geometries. Essentially, a spherical approximation is found which most closely replicates the effects of some arbitrary geometric shape. These effective sphere radii can then be used in Eq. (33) to determine the charges on the craft.

Once the charges on each craft have been determined, the electrostatic force between the craft is computed as

$$F_T = k_T \frac{q_1 q_2}{L^2}. \quad (34)$$

Note that the force acts along the line of sight vector connecting the center of the spheres. If the craft are charged to the same polarity, the force will be repulsive. If the craft are charged to opposite polarity, the force will be attractive.

## RELATIVE MOTION FEEDBACK CONTROL DESIGN AND ANALYSIS

### Nonlinear Control Development

For the relative control algorithm design, the equations of motion in the spherical frame are used. The spherical equations of motion are convenient because the  $L$  parameter corresponds directly to the separation distance between the craft. Careful actuation of the separation distance is critical, as it must be ensured that the two craft do not impact each other. Consider the state vector  $\mathbf{X} = [L \ \theta \ \phi]^T$ . With a proper control law, thrusting can be used to enforce some desired relative position of chief and deputy defined in terms of the spherical coordinates. Such a control law is developed using the candidate Lyapunov function

$$V(\mathbf{X}, \dot{\mathbf{X}}) = \frac{1}{2}(\mathbf{X} - \mathbf{X}_r)^T [K](\mathbf{X} - \mathbf{X}_r) + \frac{1}{2}\dot{\mathbf{X}}^T \dot{\mathbf{X}}, \quad (35)$$

where  $[K]$  is a positive definite gain matrix and  $\mathbf{X}_r$  is a vector containing some desired steady state values for  $L$ ,  $\theta$  and  $\phi$ . Taking the time-derivative of  $V$  yields

$$\dot{V}(\mathbf{X}, \dot{\mathbf{X}}) = \dot{\mathbf{X}}^T ([K](\mathbf{X} - \mathbf{X}_r) + \ddot{\mathbf{X}}). \quad (36)$$

Substituting Eq. (30) in for  $\ddot{\mathbf{X}}$ , the Lyapunov function rate is expressed as

$$\dot{V}(\mathbf{X}, \dot{\mathbf{X}}) = \dot{\mathbf{X}}^T ([K](\mathbf{X} - \mathbf{X}_r) + [F(L, \theta, \phi, \dot{L}, \dot{\theta}, \dot{\phi})] + [G(L, \phi)]^S \mathbf{u}). \quad (37)$$

To ensure stability, the Lyapunov function rate is set to the negative semidefinite form

$$\dot{V}(\mathbf{X}, \dot{\mathbf{X}}) = -\dot{\mathbf{X}}^T [P] \dot{\mathbf{X}}, \quad (38)$$

where  $[P]$  is a positive definite gain matrix. Selecting  $^S \mathbf{u}$  to be

$$^S \mathbf{u} = [G(L, \phi)]^{-1} \left( -[P] \dot{\mathbf{X}} - [K](\mathbf{X} - \mathbf{X}_r) - [F(L, \theta, \phi, \dot{L}, \dot{\theta}, \dot{\phi})] \right) \quad (39)$$

satisfies the negative semidefinite form in Eq. (38). While this ensures stability in the sense of Lyapunov, it does not guarantee asymptotic convergence to the desired reference location  $\mathbf{X}_r$ . To prove asymptotic convergence higher order derivatives of the Lyapunov function are used, which

are evaluated on the set  $\dot{V}(\mathbf{X}, \dot{\mathbf{X}}) = 0$ .<sup>13</sup> The closed loop response of the system with the control developed above is

$$\ddot{\mathbf{X}} + [P]\dot{\mathbf{X}} + [K](\mathbf{X} - \mathbf{X}_r) = \mathbf{0}. \quad (40)$$

The second derivative of the Lyapunov function is

$$\ddot{V}(\mathbf{X}, \dot{\mathbf{X}}) = -2\dot{\mathbf{X}}^T[P]\ddot{\mathbf{X}}. \quad (41)$$

Evaluated on the set  $\dot{\mathbf{X}} = \mathbf{0}$  (which corresponds to  $\dot{V}(\mathbf{X}, \dot{\mathbf{X}}) = 0$ ), it is clear that the second derivative of the Lyapunov function is zero. Computing the third derivative yields

$$\ddot{V}(\mathbf{X}, \dot{\mathbf{X}}) = -2\ddot{\mathbf{X}}^T[P]\ddot{\mathbf{X}} - 2\dot{\mathbf{X}}^T[P]\ddot{\mathbf{X}}. \quad (42)$$

After substituting the closed loop dynamics in Eq. (40) and evaluating on the set  $\dot{\mathbf{X}} = \mathbf{0}$ , the third derivative of the Lyapunov function is reduced to

$$\ddot{V}(\mathbf{X}, \dot{\mathbf{X}}) = -2(\mathbf{X} - \mathbf{X}_r)^T[K]^T[P][K](\mathbf{X} - \mathbf{X}_r), \quad (43)$$

which is negative definite in terms of  $\mathbf{X}$  due to the fact that both  $[K]$  and  $[P]$  are positive definite. Thus, the control law is asymptotically stabilizing. Furthermore, due to the quadratic form of both  $V$  and  $\dot{V}$ , it is concluded that the controller is globally asymptotically stabilizing.

The control acceleration  ${}^S\mathbf{u}$  contains contributions from both the inter-craft Coulomb force and the inertial thrusters on the tug satellite,

$${}^S\mathbf{u} = \begin{bmatrix} u_L \\ u_\theta \\ u_\phi \end{bmatrix} = {}^S\mathbf{F}_T \left( \frac{1}{m_T} + \frac{1}{m_d} \right) + \frac{{}^S\mathbf{T}_t}{m_T}. \quad (44)$$

Once the necessary control acceleration is known, the thrust vector is computed as

$${}^S\mathbf{T}_t = m_T \left( {}^S\mathbf{u} - {}^S\mathbf{F}_T \left( \frac{1}{m_T} + \frac{1}{m_d} \right) \right) \quad (45)$$

## Gain Selection

In order for the electrostatic force to be functional as a tether, the inertial thrust magnitude must be small enough so that the craft do not pull away from each other. With an electrostatic force magnitude on the order of milliNewtons, an inertial thruster magnitude on the order of Newtons would be too large to prevent the tug and deputy from pulling away. The thrust magnitude and electrostatic force magnitude must be on the same order. Thus, it is important to select control system gains that will result in appropriate thrust levels.

If the  $[K]$  and  $[P]$  matrices are selected to be diagonal, the closed-loop equations of motion for each of the three coordinates decouple into the form

$$\ddot{L} + P_L\dot{L} + K_L(L - L_r) = 0 \quad (46a)$$

$$\ddot{\theta} + P_\theta\dot{\theta} + K_\theta(\theta - \theta_r) = 0 \quad (46b)$$

$$\ddot{\phi} + P_\phi\dot{\phi} + K_\phi(\phi - \phi_r) = 0. \quad (46c)$$

The response of the system will mimic a simple damped harmonic oscillator. This allows for the selection of gains to control both the damped nature of the response, and the settling time. Consider the standard harmonic oscillator equations of motion,

$$\ddot{x} + 2\zeta\omega_n\dot{x} + \omega_n^2x = 0, \quad (47)$$

where  $\omega_n$  is the natural frequency of the system and  $\zeta$  is the damping coefficient. Here, a slightly underdamped response will be prescribed. To achieve this, the desired  $\zeta$  value is set at 0.925 for each of the three spherical coordinates. Correspondingly, each of the  $P_i$  gains is set at  $1.85\omega_n$ . Note that the natural frequency of each of the coordinate responses is directly controlled by the gain  $K_i$  with the relationship  $\omega_{n,i} = \sqrt{K_i}$ . The values for the gains  $K_i$  are determined by choosing a desired settling time for the system. The settling time, denoted as  $T_s$ , is the time at which the response reaches and stays within two percent of its final value. From the system dynamics, the settling time is computed as<sup>14</sup>

$$T_s = \frac{-\ln(0.02\sqrt{1-\zeta^2})}{\zeta\omega_n}. \quad (48)$$

Because of the relationship between the feedback gains  $K_i$  and the natural frequency of the system response, the necessary gain for any desired settling time can quickly be determined. For a given settling time with the slightly underdamped response specified above, the gains for the system are

$$K_i = \left( \frac{-\ln(0.02\sqrt{1-0.925^2})}{0.925T_s} \right)^2 = \frac{27.829}{T_s^2} \quad (49a)$$

$$C_i = 1.85\sqrt{K_i}. \quad (49b)$$

The effects of the settling time on the control system gains are readily apparent. As the settling time is increased, the gains will decrease. This is illustrated in Figure 3, which shows the gains necessary to achieve a variety of settling times with nearly critical damping. Note that the desired settling times are plotted as a fraction of a GEO orbital period. The rate of decrease for the  $K$  gain is higher than that of the  $P$  gain. This can be attributed to the fact that  $K$  decreases as  $1/T_s^2$ , while  $C$  decreases as  $1/T_s$ . This inversely proportional decay has important implications on thruster requirements. The necessary thrust magnitudes are directly affected by these gains; if a quick settling time is desired, the required thrust magnitudes will be much higher than those for a slower settling time. To illustrate this point, consider the required initial thrust magnitude for a particular case where the initial position errors are  $(L - L_r) = 10$  m,  $\theta = 10^\circ$ , and  $\phi = 10^\circ$ . Assuming the craft are stationary relative to each other at this epoch, the resulting control thrust magnitudes for this initial error are shown in Figure 3. The thrust magnitudes vary several orders of magnitude depending on the settling time, ranging from hundredths of a Newton to tens of microNewtons. When considering a baseline settling time to serve as the standard for the controller, this variation must be considered carefully. Once the parameters have converged to their desired values, the thrust in the L direction will converge to an order of magnitude on par with the Coulomb force acting between the two bodies, which will be on the order of milliNewtons. While thrust levels on the order of Newtons are certainly achievable, it would be very difficult to achieve a resolution accuracy down to the order of fractions of a milliNewton. For this reason, it is better to choose a settling time that will keep that maximum thrust level on the order of milliNewtons. Thrusters operating on this level should be able to achieve the resolution accuracy necessary to offset the Coulomb force once the relative craft positions converge to the desired locations. For this reason, a settling time of 0.1 orbital periods will be selected as the baseline settling time.

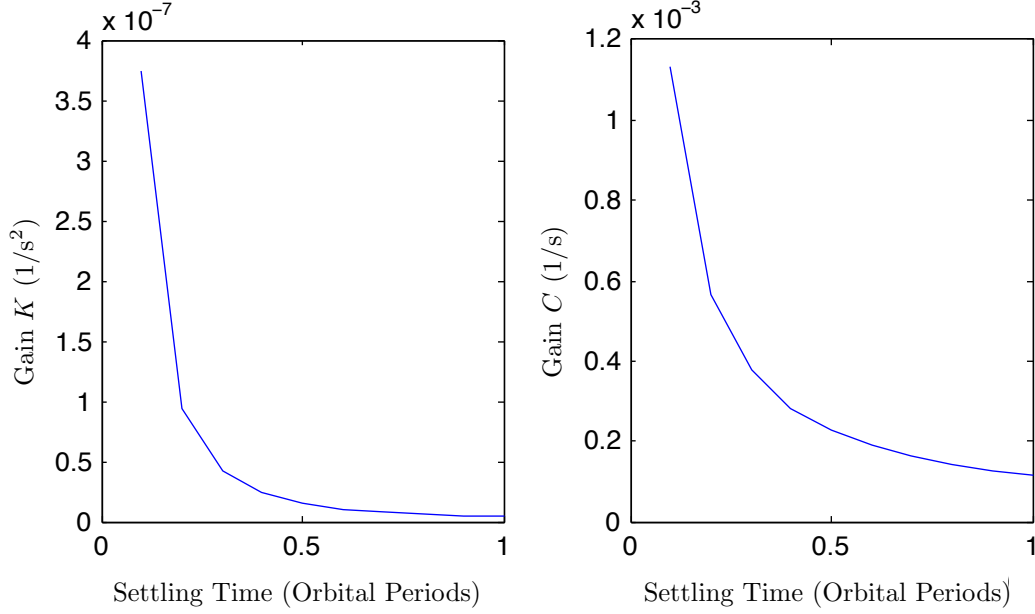


**Figure 3. Effects of settling time on control system gains.**

### Uncertainties in Craft Charges

The control system formulation assumes that the charges on the craft are known exactly. Naturally, it is of interest to determine the effects on the control system response when the craft charges are modeled imperfectly. This is an important consideration because in actual implementation, the charges will not be known precisely. When the charges are not modeled correctly, the closed loop response of the control system for the separation distance  $L$  is

$$\ddot{L} + P_L \dot{L} + K_L(L - L_r) = \frac{k_T}{L^2}(Q_{12} - Q_{12e}) \left( \frac{1}{m_T} + \frac{1}{m_d} \right), \quad (50)$$

where  $k_T$  is Coulombs constant,  $Q_{12}$  is the actual charge product ( $q_1 q_2$ ) of the two craft, and  $Q_{12e}$  is the estimated charge product implemented in the controller. It is desired to obtain information about where the equilibrium separation distance is with improperly modeled charges. To do so, the equilibrium conditions  $\ddot{L} = \dot{L} = 0$  are applied. For compactness of notation, introduce

$$\mu = k_T \left( \frac{1}{m_T} + \frac{1}{m_d} \right) \quad (51a)$$

$$\Delta Q = (Q_{12} - Q_{12e}). \quad (51b)$$

The closed loop equilibrium positions are found by solving

$$K_L(L - L_r) = \frac{\mu}{L^2} \Delta Q.$$

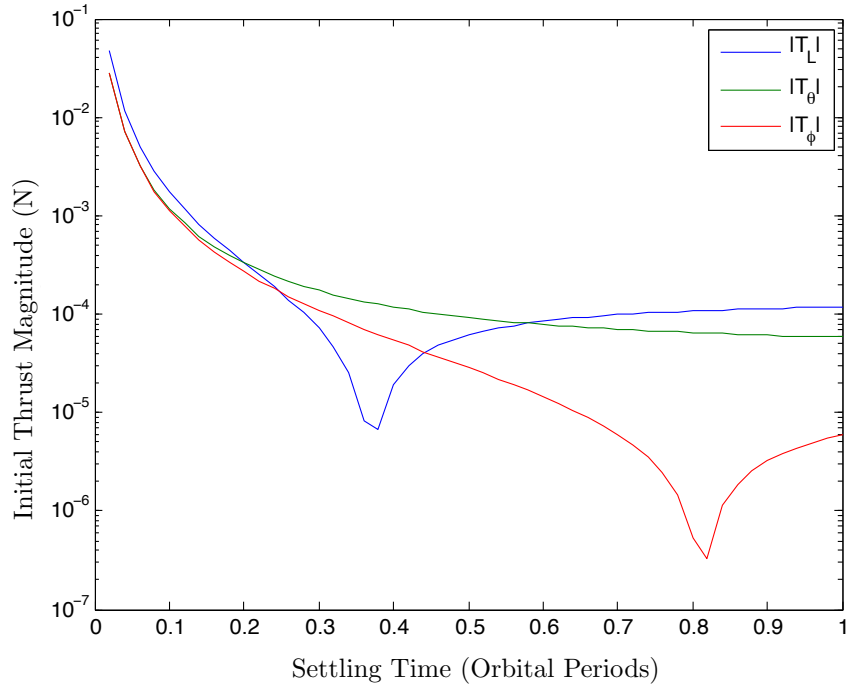


**Figure 4.** Effects of settling time on initial thrust magnitudes for errors of  $(L - L_r) = 10 \text{ m}$ ,  $\theta = 10^\circ$ , and  $\phi = 10^\circ$ .

With minor rearranging, a third order polynomial is obtained,

$$K_L L^3 - K_L L_r L^2 - \mu \Delta Q = 0 \quad (52)$$

The roots of this polynomial yield the equilibrium separation distance of the deputy relative to the chief. Note that only positive  $L$  values are realizable, based on the way the coordinate frame is defined. Because the  $L$ -direction is defined from the deputy to the chief, a negative  $L$  value can never be obtained. Thus, we are concerned only with the existence of positive roots of the polynomial. The existence of such roots can be determined using Descartes rule of signs.

The sign of  $\Delta Q$  plays an important role in determining the existence of positive roots. First, consider the case when the control system over-predicts the craft charges. That is, the actual magnitudes of the craft charges are smaller than implemented in the control system. When this is the case,  $\Delta Q$  will be positive. In the polynomial, only one sign change will occur between the  $L^3$  and  $L^2$  terms. As a result, it is certain that there will be one positive root, meaning the control system will drive the system to a positive  $L$  value. The magnitude of this equilibrium  $L$  is dependent on the feedback gain, the charges, and the craft masses.

Different behavior is obtained when the charges are under-predicted. When the controller assumes smaller charge magnitudes than the craft actually experience,  $\Delta Q$  is negative. Now, the polynomial will have two sign changes. This means that there will be either zero or two real positive roots. The possibility of no equilibria is intriguing, as it implies the control system may fail to prevent a collision between the deputy and chief. To determine at which point the transition between zero and two positive roots occurs, the condition where Eq. (52) and its derivative both equal zero

simultaneously is considered. The derivative of (52) taken with respect to  $L$  is

$$3K_L L^2 - 2K_L L_r L = 0, \quad (53)$$

which has a root at

$$L = \frac{2}{3}L_r. \quad (54)$$

Plugging this value back into the original polynomial yields the necessary gain that will ensure the existence of positive real roots. In order to ensure that an equilibrium exists in the closed loop system response, it is required that

$$K_L \geq \frac{27\mu|\Delta Q|}{4L_r^3}. \quad (55)$$

Interestingly, the requirement on the gain is dependent on the reference separation distance,  $L_r$ , and the error in the charge requirements. The required gain actually decreases with the cube of the reference distance. As a result, much higher gains are needed to ensure an equilibrium exists when the craft are desired to fly close than when they are desired to fly far apart. In order to properly bound  $K_L$ , some knowledge is needed regarding what errors may be expected in the estimation of the craft charges.

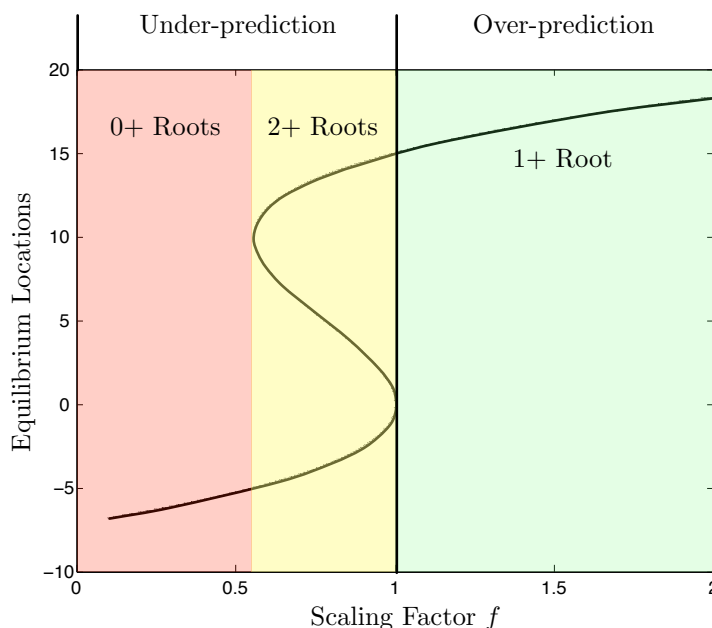


**Figure 5. Effects of sweeping scaling parameter  $f$  on equilibrium locations.**

To illustrate the importance of proper gain selection, equilibrium locations are determined for an example case as a function of uncertainty in the craft charges. To provide a scalable parameter representative of the severity of under- or over-prediction, the estimated charge product is defined as

$$Q_{12e} = fQ_{12}, \quad (56)$$

**Table 1. Initial spherical coordinates used in simulation**

$L$	$\theta$	$\phi$	$\dot{L}$	$\dot{\theta}$	$\dot{\phi}$
37.03 m	-34.12°	15.67°	$5.97 \times 10^{-7}$ m/s	$1.58 \times 10^{-7}$ °/s	$-2.58 \times 10^{-7}$ °/s

where  $f$  is a positive scaling parameter. When  $f$  is greater than one, the charges are overpredicted. When  $f$  is less than one, under-prediction occurs. For this study, the charge product is assumed to be  $Q_{12} = -2.5 \times 10^{-11}$  C. The reference separation distance is set at  $L_r = 15$  m, and the masses are  $m_d = 500$  kg and  $m_T = 2000$  kg. Assuming a feedback gain of  $K_L = 5 \times 10^{-7}$ , the scaling parameter  $f$  is swept from under-prediction to over-prediction, and the real equilibria are computed for each  $f$  value. The results are shown in Figure 5. The plot is divided into two main regions. The first is  $f > 1$ , which corresponds to the controller over-predicting the craft charges. As expected, only one equilibrium exists in this region. As the over-prediction becomes more severe, the location of the equilibrium configuration moves further and further away from the desired nominal position of  $L = 15$  m. Note that when  $f = 1$ , the equilibrium falls exactly at 15 m. This corresponds to perfect prediction of the craft charges by the controller. When  $f < 1$ , the controller is under-predicting the actual craft charges. The region of under-prediction is subdivided into two different cases: one with two positive roots, and one with zero positive roots. As  $f$  decreases from one, the larger equilibrium location decreases from 15 meters, and a new equilibrium appears at  $L = 0$  m. This new equilibrium grows from zero as the underprediction becomes more severe, until it collides with the larger equilibrium and vanishes at approximately  $f = 0.55$ . Note that the larger equilibrium value is stable, while the lower one is unstable. When  $f$  is lower than this value, no positive equilibria exist. This is a dangerous region to be in, as the craft may impact if nothing is done to prevent a collision.

The example shown here is not intended to represent a specific operational scenario. Rather, the parameters used to generate the plot were chosen in order to demonstrate all of the possible behavior that may occur when the charges are improperly modeled. Practically, the gain should be increased to a level where there is no region in  $f$  with zero positive roots. As  $K_L$  increases, the width of the yellow region in Figure 5 will increase as well. Likewise, this region will shrink when  $K_L$  is decreased. It is advantageous to make this region as large as possible, as it provides a wider allowable margin of error in predicting the craft charges.

The preceding results are obtained assuming the craft charges are fixed with time. This assumption is made in order to provide analytical insight into the issue of improperly modeled charges. In the actual system model, the charges change as the distance between the bodies evolves. Unfortunately, including this behavior in the analytical developments precludes the existence of useable insight. Qualitatively, however, the behavior is the same. The preceding developments provide a starting point for proper gain selection and potential outcomes that may occur with improperly modeled charges.

## NUMERIC SIMULATION

To illustrate the performance of the developed control system, inertial simulations are used. Rather than integrating the linearized spherical equations of motion, the full nonlinear equations of motion, presented as Eqs. (11) and (12), are used. The linearized control developed with spherical coordinates is used to determine  $u_T$ . The control system is used to raise the semi-major axis

**Table 2. Parameter values used in numeric simulation**

Parameter	$m_T$	$m_d$	$V_T$	$V_d$	$R_T$	$R_d$
Value	500 kg	2000 kg	25 kV	-25 kV	2 m	3 m

of the deputy orbit by 300 km, starting at a geosynchronous orbit radius of 42,164 km. Such a scenario is representative of raising a GEO debris object into a super-geosynchronous disposal orbit. To begin the simulation, the deputy is placed in a circular orbit with radius 42,164 km. The relative spherical coordinates between the deputy and chief at epoch are shown in Table 1. The parameter values used in the simulation are summarized in Table 2. The simulation is run until an increase in the semi-major axis of 300 km is achieved.

For the simulation, the control algorithm is implemented assuming perfect knowledge of the state and craft voltages. The electrostatic force model described in Eq. (34) is used to model the effects of the craft charging by means of the position-dependent capacitance model in Eq. (33). Note that the craft voltages, presented in Table 2, are held constant throughout the simulation. The charges vary as the relative positions of the craft change during the maneuver according to Eq. (33).

For comparison, a simulation is run where the electrostatic force is not modeled properly; rather, over-prediction of 10% in the force magnitude is considered. Because the electrostatic force is a direct function of the charge product of the craft, this is akin to over-predicting the charge product by 10%. The same parameter values are maintained for both simulations. The case with force over-prediction is run for the same length of time as the perfect-knowledge simulation. Considering the analytical developments in the preceding section, it is expected that this scenario will result in an increase in the separation distance between the craft at steady state relative to the desired nominal position.

In the control system, desired values of the spherical coordinates are needed. The target values will affect the maneuver in several different ways. Considering first the effects of the separation distance  $L$ , the maneuver time can be significantly impacted. The thrust magnitude at steady state implemented on the tugging craft is a direct function of the electrostatic force between the craft. If the craft are 5 meters apart, for example, this force is significantly larger than if the craft are 50 meters apart. Because the thrust is a direction function of the electrostatic force, larger thrust magnitudes are possible when the craft are held at smaller separation distances. Larger thrust magnitudes enable the semi-major axis of the orbit to be increased at a more rapid rate. These effects are described in further detail in Reference 10, where Gauss' variational equations are used to determine how quickly a deputy object's semi-major axis may be increased using electrostatic forces. Next, the effects of the angles  $\theta$  and  $\phi$  are considered. When both of these angles are held at zero, the deputy will follow the chief in the orbit track. When  $\theta$  is non-zero and  $\phi$  is zero, both deputy and chief occupy the same orbit plane. In this case, planar orbit maneuvers are possible, where the deputy orbit semi-major axis, eccentricity, and argument of perigee may be modified. When  $\phi$  is non-zero, the deputy and chief are no longer in the same orbit plane. In this configuration, the deputy orbit inclination and right ascension of the ascending node may be modified, in addition to the other orbital elements. In the current study, a planar orbit raising maneuver is considered. As such, the values targeted by the controller are set at  $L=12.5$  meters,  $\theta = \phi = 0^\circ$ . Note that this corresponds to the chief at 12.5 meters ahead of the deputy in the along-track direction.

To achieve the desired semi-major axis increase, slightly more than 61 days are required when

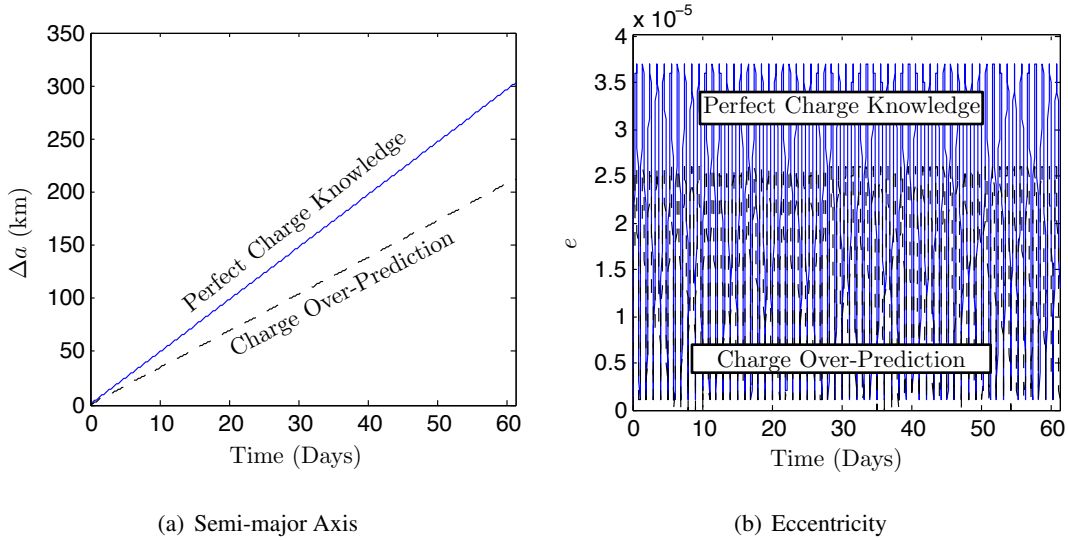


**Figure 6. Changes in a) semi-major axis and b) eccentricity of deputy object throughout the maneuver.**

perfect knowledge of the electrostatic force is available. During the same 61 day period, the 10% error in the electrostatic force magnitude leads to an increase in the semi-major axis of only 211.6 km. The evolution of the semi-major axis and eccentricity of the deputy object during the maneuver is shown in Figure 6. Note that the increase in the semi-major axis is shown, and the trend is linear. This is attributed to the fact that a constant force is applied to the deputy object in the along track direction. As such, the rate of increase in the semi-major axis is nearly constant throughout the duration of the maneuver. The eccentricity spikes early on in the maneuver, then oscillates for the remainder. This early spike can be attributed to the initial maneuvering of the chief relative to the deputy. During this early repositioning the force on the deputy is not constant in magnitude or direction, as the electrostatic force between the craft is changing. Once the steady state relative position is achieved, the force becomes constant and the oscillation results. The decreased performance in the case of force over-prediction is attributed to the steady state conditions achieved by the controller. When this force is over-predicted, the craft settle into a separation distance larger than when the force is known perfectly. As a result the tugging force is smaller, which leads to a lower rate of change for the semi-major axis.

Initially, the deputy and chief are not in the desired relative position. There is a repositioning of the chief relative to the deputy during the early portion of the maneuver. This is illustrated by considering the evolution of the spherical coordinates during the first 12 hours, shown in Figure 7. Using the gain-selection process detailed previously, gains are chosen so that the settling time for the system is 0.1 days ( $K = 3.7484 \times 10^{-7} \text{ 1/s}^2$  and  $C = 1.1327 \times 10^{-3} \text{ 1/s}$ ). The response of the system using these gains reveals the desired settling time has been achieved. A slightly underdamped response is obtained before the chief settles into its steady-state relative position. When the electrostatic force is modeled exactly, the target is achieved. When the force is over-predicted by 10%, the desired angles are achieved but the separation distance increases to about 15 m. Once steady-state is achieved in both cases, the relative position is held throughout the duration of the maneuver. Recall that inertial simulations are used during these simulations. The spherical

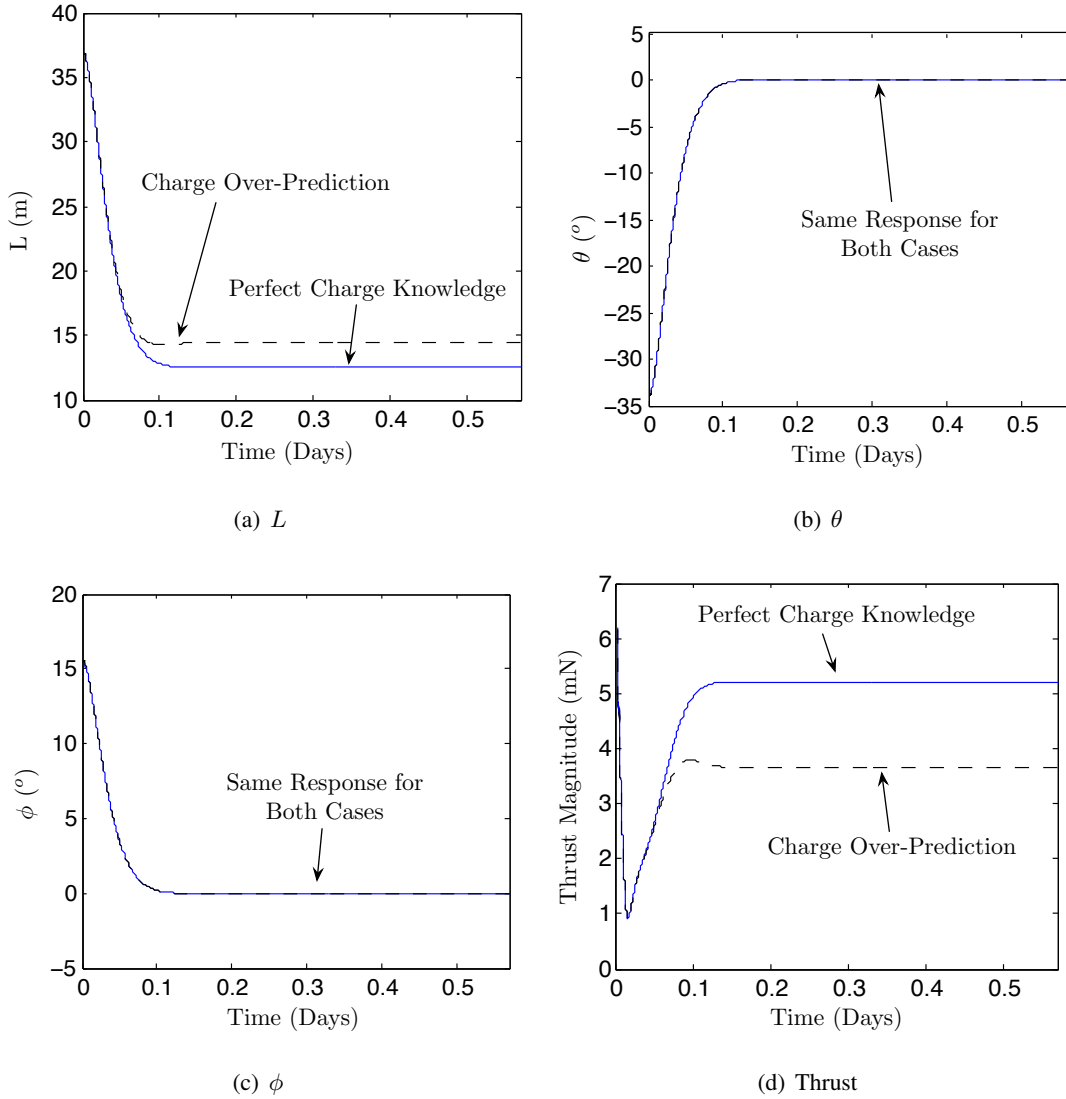


**Figure 7. Evolution of spherical coordinates a)  $L$  b)  $\theta$  and c)  $\phi$  and d) magnitude of chief thrust during the first 12 hours of the maneuver for perfect charge knowledge and over-prediction of charge product by 10%.**

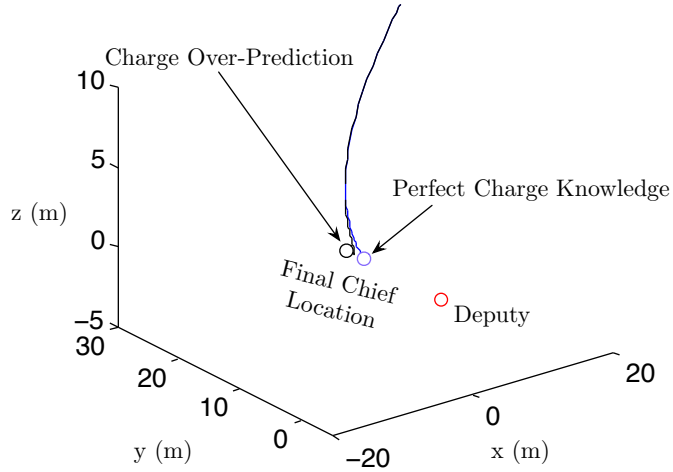


**Figure 8. Relative motion of chief with respect to deputy (in Hill frame) for perfect charge knowledge and over-prediction of charge product by 2.5%.**

coordinates shown here are obtained by computing the relative position of the craft and then rotating the result into the appropriate coordinate frame.

Inspection of the spherical coordinate histories reveals the differences in performance between the two simulated cases. For both simulations the settling time is the same, as are the histories for the angles  $\theta$  and  $\phi$ . This is due to the decoupling between the coordinates in the control system. In spherical coordinates, the electrostatic force is only present in the  $L$ -direction. Thus, the feedback compensation for the electrostatic force will directly affect only this direction. Indirect effects are present in the dynamics due to the coupling of the coordinates in the equations of motion. The control system, however, effectively removes this decoupling by compensating for these dynamics in the control algorithm. Thus, errors in the electrostatic force model will manifest predominately in the  $L$ -direction with minimal deleterious effects on the desired response for the angles. Still, errors in the electrostatic force model can cause serious concerns. Here, over-prediction is considered. In this scenario, the primary effect is that the desired semi-major axis increase will take longer. A potentially more problematic scenario is when the electrostatic force is under-predicted. If the controller assumes the magnitude of the electrostatic force is less than it really is, the two craft could collide.

The magnitude of the thrust on the chief craft is shown in Figure 7(d) for the first part of the maneuver. Beyond this initial period, the magnitude remains constant at the steady value indicated on the plot. Note that the steady state value is lower for the charge over-prediction case. This corresponds to the fact that the steady-state separation distance is larger for the charge over-prediction case. As a result, the thrusters do not need as large a magnitude to compensate for the lower electrostatic force than they do when the craft are closer. The effect that this has on the overall maneuver is a lower tugging force which, in turn, does not increase the semi-major axis as readily as the case when the electrostatic force is modeled perfectly.

The relative trajectory of the chief with respect to the deputy in the Hill frame is shown in Figure 8 for both cases. The approach trajectory from the initial condition is nearly identical for the case of perfect charge knowledge and charge over-prediction. This is largely due to the same angle history

achieved by the controller for both histories (see Figure 7). For a large duration of the repositioning, the separation distance history is very similar as well. It is only when the craft are within 15 meters of each other that a deviation occurs. Recall that once steady-state is achieved the relative positions of the craft remain constant in the Hill frame.

## CONCLUSION

In this paper, an autonomous relative navigation control algorithm is proposed for the case when two charged spacecraft are in close proximity of each other. Denoting one craft as the chief and the other as the deputy, thrust is applied to the chief to reposition it into a desired relative position with respect to the deputy. The electrostatic force generated between the craft is then used as a contactless tug which enables the chief to tow the deputy into a different orbit. Here, a planar orbit raising maneuver is simulated to test the control algorithm, and improperly modeled charges are considered. The control algorithm demonstrates its validity by successfully repositioning the chief and achieving an increase in the deputy semi-major axis of 300 km using an electrostatic tugging force. When the charges are not modeled properly in the controller, the chief settles into a separation distance slightly larger than desired. This has minimal impact on the targeted mission, however; the only significant difference between the cases is the time needed to achieve a semi-major axis increase of 300 km. The electrostatic tug concept has been validated as a viable means for reorbiting space objects.

## REFERENCES

- [1] L. B. King, G. G. Parker, S. Deshmukh, and J.-H. Chong, "Spacecraft Formation-flying using Inter-vehicle Coulomb Forces," tech. rep., NASA/NIAC, <http://www.niac.usra.edu>, January 2002.
- [2] L. B. King, G. G. Parker, S. Deshmukh, and J.-H. Chong, "Study of Interspacecraft Coulomb Forces and Implications for Formation Flying," *AIAA Journal of Propulsion and Power*, Vol. 19, No. 3, 2003, pp. 497–505.
- [3] L. Pettazzi, D. Izzo, and S. Theil, "Swarm navigation and reconfiguration using electrostatic forces," *7th International Conference on Dynamics and Control of Systems and Structures in Space*, The Old Royal Naval College, Greenwich, London, England, 16-20 July 2006.
- [4] A. Natarajan and H. Schaub, "Hybrid Control of Orbit Normal and Along-Track Two-Craft Coulomb Tethers," *Aerospace Science and Technology*, Vol. 13, June–July 2009, pp. 183–191.
- [5] C. R. Seubert and H. Schaub, "Tethered Coulomb Structures: Prospects and Challenges," *Journal of the Astronautical Sciences*, Vol. 57, Jan.–June 2009, pp. 347–368.
- [6] C. R. Seubert, S. Panosian, and H. Schaub, "Dynamic Feasibility Study of a Tethered Coulomb Structure," *AAS/AIAA Astrodynamics Specialist Conference*, Toronto, Canada, Aug. 2–5 2010.
- [7] S. Wang and H. Schaub, "Nonlinear Charge Control for a Collinear Fixed Shape Three-Craft Equilibrium," *AIAA Journal of Guidance, Control, and Dynamics*, Vol. 34, Mar.–Apr. 2011, pp. 359–366.
- [8] S. Wang and H. Schaub, "Switched Lyapunov Function Based Coulomb Control of a Triangular 3-Vehicle Cluster," *AAS/AIAA Astrodynamics Specialist Conference*, Pittsburgh, PA, Aug. 9–13 2009.
- [9] H. Schaub, G. G. Parker, and L. B. King, "Challenges and Prospects of Coulomb Spacecraft Formation Control," *Journal of the Astronautical Sciences*, Vol. 52, No. 1-2, 2004, pp. 169–193.
- [10] H. Schaub and D. F. Moorer, "Geosynchronous Large Debris Reorbiter: Challenges and Prospects," *AAS Kyle T. Alfriend Astrodynamics Symposium*, Monterey, CA, May 17–19 2010.
- [11] H. Schaub and J. L. Junkins, *Analytical Mechanics of Space Systems*. Reston, VA: AIAA Education Series, 2nd ed., October 2009.
- [12] W. R. Smythe, *Static and Dynamic Electricity*. McGraw-Hill, 3rd ed., 1968.
- [13] R. Mukherjee and D. Chen, "Asymptotic Stability Theorem for Autonomous Systems," *Journal of Guidance, Control, and Dynamics*, Vol. 16, 1993, pp. 961–963.
- [14] N. S. Nise, *Control Systems Engineering*. Wiley, 5th ed., 2008.